Journal of Environmental Chemical Engineering 10 (2022) 107366

Contents lists available at ScienceDirect

Journal of Environmental Chemical Engineering

journal homepage: www.elsevier.com/locate/jece

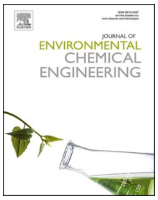

Activation of peroxydisulfate by bimetal modified peanut hull-derived porous biochar for the degradation of tetracycline in aqueous solution

Yuan Pan [1], Zan Peng [1], Zhifeng Liu *, Binbin Shao, Qinghua Liang, Qingyun He, Ting Wu, Xiansheng Zhang, Chenhui Zhao, Yang Liu, Lin Ge, Miao He

College of Environmental Science and Engineering, Hunan University and Key Laboratory of Environmental Biology and Pollution Control (Hunan University), Ministry of Education, Changsha 410082, PR China

ARTICLE INFO

Editor: Dr. G. Palmisano

Keywords:
Advanced oxidation process
Organic pollutants
Peroxydisulfate
Biochar
Bimetal modification
Porous structure

ABSTRACT

The sulfate radical-based advanced oxidation processes (SR-AOPs) are considered to be efficient and environmentally friendly for handling persistent organic pollutants issues. The activation of persulfate (PS) by biochar (BC) materials derived from waste biomass is the current research hotspot in SR-AOPs. Herein, we propose bimetal modified peanut hull-derived biochar (BC-Fe-1-Zn) catalysts to activate PS to degrade tetracycline (TC) with a removal efficiency of 90% in 120 min. The physicochemical properties and reaction mechanisms are well studied through the effective combination of various characterization techniques and experiments. $SO_4^{\bullet-}$, $^{\bullet}OH$ and electron transfer are all involved in the degradation of TC and $SO_4^{\bullet-}$ is the main reactive oxygen species (ROSs). The Fe and Zn oxides and the oxygen-containing functional groups on the catalyst surface are considered as the active sites for the reaction. Moreover, the influences of different factors (such as pH, catalyst dosage, PS dosage and coexisting ions) on the TC remove efficiency are studied. Simultaneously, the TC degradation products and its reasonable degradation paths are analyzed. This work provides new ideas for the rational design of biochar-supported bimetallic catalysts and revealed that using BC-Fe-1-Zn in AOPs technology to environmental remediation is a promising approach.

1. Introduction

The widespread use of various pharmaceutical and personal care products (PPCPs) has caused the continuous increase of organic refractory pollutants (e.g. antibiotics) in the environmental system [1–5], it is urgent to develop efficient, economical and environmentally friendly strategies to handle this intractable issue. In recent decades, advanced oxidation technologies (such as photocatalysis [6–11], electrocatalysis [12–14], Fenton or Fenton like reaction [15], persulfate advanced oxidation process [16–18], etc.) based on free radical reaction have shown great potential in environmental remediation. Among them, the sulfate radical-based advanced oxidation processes (SR-AOPs) have been extensively studied due to its robust oxidizing effect (redox potential 2.60–3.10 V_{NHE}), wide applicable pH range (2–10), safe storage and convenient transportation [18].

Generally, persulfate can generate sulfate radicals ($SO_4^{\bullet-}$) with strong oxidizing ability only after being activated (O—O bond break). The activation mechanisms usually include external energy activation [19], metal activation [20], and carbon-based material activation [19,21] etc. However, the first two methods have been controversial on account of enormous energy consumption and secondary pollution problems. Fortunately, carbon-based materials show extraordinary potential in activating persulfate with the merits of excellent physicochemical properties, robust stability, tunable electronic structure, and environmental friendliness [18]. In particular, the activation of persulfate by biochar (BC) materials derived from waste biomass is the current research hotspot in SR-AOPs, which is attributed to the low cost and wide feedstock source as well as unique properties of BC, such as rich surface functionality and minerals [19,22]. For instance, Wang et al. found that sewage sludge-derived biochar could effectively activate peroxymonosulfate (PMS) to produce $SO_4^{\bullet-}$ to degrade triclosan [23]. Fang et al. reported that biochar-derived from pine needles could be an effective candidate for persulfate activation in SR-AOPs, and possessed outstanding effect on the removal of polychlorinated biphenyl [24].

---

* Corresponding author.
E-mail address: zhifengliu@hnu.edu.cn (Z. Liu).

[1] The authors contribute equally to this paper.

https://doi.org/10.1016/j.jece.2022.107366
Received 7 December 2021; Received in revised form 3 February 2022; Accepted 8 February 2022

Moreover, different biochar activates persulfate in different ways with generates various reactive oxygen species (ROS). Peanut hull-derived biochar (PHBC) has attracted attention due to its large specific surface area and high carbon content. Liang et al. discussed the differences in the mechanism of PHBC and activated carbon catalyzing the degradation of sulfamethoxazole by persulfate [25]. However, the efficiency of a bulk biochar to activate persulfate is not satisfactory, and the internal mechanism of reaction needs to be further explored. Recently, Wang et al. studied degradation of nitrochlorobenzene by activated persulfate oxidation with PHBC supported nanoscaled zero valent iron [26]. The synergistic effect of transition metal and biochar can strengthen the activation of persulfate and achieve the best pollutant removal efficiency. Furthermore, it is necessary to further explore the mechanism and reactive pathway of this synergistic effect. Zinc-containing substances are considered to be effective and low-cost modified agents for improving the pore structure, increasing the surface area [27]. As the common modifier, $ZnCl_2$ is helpful to activate functional groups and form ZnO nano-particles on biochar [28]. Previous study indicated that Zn could help form hydroxyl groups on the surface of the ZnO particles during the preparation process [29], moreover, the specific surface area and total porosity of zinc oxides modified biochar is increased due to the dehydration effect of zinc oxides [30]. It can also lead to the increase of hydrophobic/hydrophilic sites on the modified biochar surface [31]. Whether changing the physical structure or activating functional groups will provide active sites to improve the removal efficiency of pollutants and functionalized properties of materials. However, to the best of our knowledge, application and effect of iron-zinc bimetallic oxide (Fe-Zn) modified peanut hull-derived biochar activated persulfate in the remediation of tetracycline (TC)-contaminated water has not been reported, furthermore, the degradation mechanism of TC on Fe/Zn biochar activated persulfate system remain unclear. Such information is critical for developing AOPs with the assist of biochar to efficiently treat the antibiotics contaminated water.

Herein, we use peanut hull as raw materials to prepare biochar (BC) by pyrolysis process, then the novel bimetal modified biochar composite material (BC-Fe-1-Zn) is synthesized by the facile co-precipitation method. First of all, incorporating the transition metal Fe to BC greatly improves the electron transfer ability [31,32]. And then the pore-forming ability of $ZnCl_2$ further improves the specific surface area and porosity of the catalyst. At the same time, Zn is loaded on the catalyst surface to provide more active sites, which can further enhance the electron transfer, thereby improving the degradation performance of TC by activated peroxydisulfate (PDS) oxidation with BC-Fe-1-Zn. Moreover, the formed iron oxide particle on the catalysts is magnetic, which is conducive to the recovery and secondary utilization of the catalyst. Based on the results of morphology and chemical state analysis, reactive free radicals detection as well as electrochemical measurement, the possible degradation mechanism of TC over the BC-Fe-1-Zn is proposed. Consequently, we reasonably believe that this work will bring inspiration for the design of novel catalysts for advanced oxidation processes based on biochar.

2. Experimental section

2.1. Materials and chemicals

In this study, peanut hulls were selected as the precursors of biochar synthesis, which were purchased from Lianfeng agricultural products deep processing on the internet. Potassium peroxydisulfate ($K_2S_2O_8$), tetracycline hydrochloride (TC), sodium nitrate ($NaNO_3$), sodium sulfate (Na_2SO_4), sodium chloride (NaCl), hydrochloric acid (HCl), sodium hydroxide (NaOH), methanol (MeOH), ethanol (EtOH), sodium azide (NaN_3), tert-butanol (TBA), p-benzoquinone (p-BQ) were purchased from Sinopharm Chemical Regent Co. Ltd (Shanghai, China). All the chemicals were used directly without further purification. The experimental water was deionized water (18.25 MΩ cm^{-1}) from ultrapure (UPRII-10T) laboratory water system.

2.2. Preparation of catalysts

2.2.1. Preparation of peanut hull-derived biochar (BC)

All the raw reagents used here were of analytical grade and without further purification. The peanut hulls used in this experiment were purchased from Jinhua, Zhejiang. Firstly, the peanut hulls were placed in a blast drying box and dried at 60 °C for 12 h, and then the dried peanut hulls were crushed with a crusher and passed through a 50-mesh sieve. And then put the prepared peanut hull biomass in a plastic bag for storage. Next, took 5 g of peanut hull powder and placed it into a quartz boat which placed in tube furnace, and then under N_2 atmosphere the BC was obtained by the thermal pyrolysis of peanut hulls on the quartz boat at 700 °C for 2 h with a heating rate 5 °C min^{-1}. Finally, the dehydrated peanut hull-derived biochar was ground through a 50-mesh sieve and stored in a sealed bag for later use.

2.2.2. Preparation of BC-Fe-1-Zn composite sample

According to previous studies, the BC-Fe composite material was prepared by the co-precipitation method [33]. First, put 5 g of peanut hull biomass into a beaker with 100 mL of ultrapure water, then took a certain amount of $Fe(NO_3)_3$ into the beaker, and mix them evenly under the action of a magnetic stirrer. Next, the above solution was aged for 12 h, washed alternately 3 times with 50% ethanol and ultrapure water until the washing solution was neutral, then vacuum dried at 80 °C for 12 h, the dried mixture ground and passed through a 50-mesh sieve. Finally, the mixed biomass material was pyrolyzed in a tube furnace to obtain BC-Fe samples. In this study, BC-Fe composite materials with different mass ratios (10%, 20%, 30%, 40%) were prepared, in which the amount of peanut hull biomass was fixed at 5 g, and the mass of $Fe(NO_3)_3$ was 0.5 g, 1.0 g, 1.5 g, 2.0 g, respectively, corresponding sample is denoted as BC-Fe-x (x = 0, 0.5, 1.0, 1.5 and 2.0).

The preparation method of the BC-Fe-1-Zn composite material was the same as above, mixing 1 g $ZnCl_2$ with 5 g peanut hull biomass and 1 g $Fe(NO_3)_3$ uniformly, then aging, washing, drying, grinding, sieving and pyrolysis. Finally, the prepared materials were marked, put in a sealed bag and stored in a dry box for further use.

2.3. Characterization

The microstructures and morphologies of as-prepared samples were investigated by scanning electron microscopy (SEM, Zeiss Gemini 300). X-ray diffraction (XRD, German Bruker AXS D8 Advance) was used to explore the crystal phase of samples with a Cu-Kα source ($\lambda = 1.5406$ Å) operated at 40 kV and 40 mA. The surface chemical compositions and valence states were surveyed by X-ray photoelectron spectroscopy (XPS, Thermo Scientific K-Alpha). The Brunauer-Emmett-Teller (BET) method through an analytical instrument (Quantachrome Quadrasorb SI, United States) was used to test the specific surface areas and pore distribution of the samples. Fourier transform infrared (FTIR) spectra were conducted by a KBr tableting method on a Nicolet iS10 spectrometer (Thermo Scientific, United States). Zeta potential was detected by a Zetasizer Nano ZS (Malvern, UK). A vibrating sample magnetometer (VSM, LakeShore7404, USA) was used to test the magnetic hysteresis loops of BC-Fe-1-Zn catalyst.

2.4. Measurements of catalytic TC degradation

All reaction experiments involved in this study were carried out in a 200 mL flask. In a representative process, 100 mL of TC solution (20 mg L^{-1}) containing 1 g L^{-1} catalysts samples was prepared, after ultrasonic dispersion for 10 min, the obtained suspension solutions were continuously stirred to achieve the adsorption-desorption equilibrium, then 2 g L^{-1} PDS was added at 25 ± 1.0 °C, the pH of the initial reaction was maintained at 7. Subsequently, at certain time intervals, 1 mL of the suspension was collected. After removing the catalyst sample powder by centrifugation and filtration with a millipore filter (0.45 μm) and mixed with 1 mL methanol for quenching residual free radicals. Under the same experimental procedures, the effects of pH conditions (pH = 3, 5, 7, 9, 11), catalyst samples dosage (0.25, 0.5, 1.0, 2.0 g L^{-1}), PDS concentration (0.5, 1.0, 2.0, 3.0 g L^{-1}), and different anions species (NO_3^-, Cl^-, SO_4^{2-}) on the TC degradation were investigated. The concentration of the TC was determined using an UV–vis spectrophotometer at the absorption peak of 357 nm.

2.5. Electrochemical measurements

The electrochemical impedance spectroscopy (EIS) and transient photocurrent of as-prepared samples were performed on a Chenhua CHI 760E workstation in a three-electrode system. An Ag/AgCl electrode and a Pt electrode were used as the reference and counter electrode, respectively. Generally, via a simple drop-casting method for working electrode preparation: 5.0 mg of as-prepared sample was dispersed in 1.0 mL of 0.5% nafion solution and ultrasonicated for 1 h. Then, a certain amount of the above suspension was dripped onto fluorine-doped tinoxide (FTO) glass (1 × 1 cm^2) which was ultrasonic pre-cleaned with acetone, ethanol and deionized water, respectively. Subsequently, the working electrode was dried in an oven to form a film. The obtained electrode was dried at 80 °C for 4 h, and then calcined at 120 °C for 1 h. The EIS was tested on an applied voltage of 0.2 V with amplitude of 0.05 V over a frequency between 10^{-2} and 10^5 Hz. The EIS of the samples were tested in Na_2SO_4 (0.2 mol L^{-1}) electrolyte solution. The linear sweep voltammetry (LSV) curves were measured in an O_2-saturated phosphate buffer solution (0.1 mol L^{-1}, pH = 7) containing 2 g L^{-1} PDS and 20 mg L^{-1} TC with a scan rate of 5 mV s^{-1}.

2.6. Analysis methods

The degradation intermediates of TC were identified by a LC-MS/MS system (1290/6460 Triple Quad, Agilent) equipped with a Kromasil C18 column (250 × 4.6 mm, 5 μm). The elution was performed via 0.1% (v/v) of formic acid aqueous solution (A) and acetonitrile (B) at a flow rate of 0.3 mL min^{-1}. The injection volume was 2 μL, and the column temperature was 30 °C.

The electron paramagnetic resonance (EPR) spectra were monitored using a EPR spectrometer (Bruker EMXnano, Germany) with Microwave Bridge (microwave frequency 9.83 GHz; microwave power, 22.8 mW; modulation amplitude, 1 G; modulation frequency, 100.00 kHz), where 5,5-dimethyl-1-pyrrolidine-N-oxide (DMPO) or tetramethylpiperidine (TEMP) was used as the spin-trapping agent.

3. Results and discussion

3.1. Morphology, crystal structure, and chemical state analysis

The morphologies of as-prepared samples were characterized with SEM, and used EDS to analyze the elements contained in the catalyst samples. Fig. 1, Fig. S1 and Table S1 displayed the SEM images and EDS analysis data of BC, BC-Fe-1 and BC-Fe-1-Zn samples, respectively. Evidently, BC is in the form of flakes with a porous structure (Fig. 1A), and the surface is relatively rough. The carbon and oxygen content of the unmodified peanut hull-derived biochar reaches 98.81% and 1.02%, respectively, and the EDS energy spectrum (Fig. S1) analysis shows that the peanut hull-derived biochar originally contains trace metal elements of iron and zinc, which may be due to the peanut hulls absorbing metal elements in the soil. There are granular substances on the surface of BC-Fe-1 (Fig. 1B), from the EDS analysis data (Table S1), it can be seen that the weight ratio of iron in the composite material has increased from 0.43% to 2.06% and the atomic ratio is 0.48%, indicating that the iron ions have successfully adhered to BC surface. As shown in Fig. 1C, a large pore size can be found on the surface of BC-Fe-1-Zn samples. The real loading of Fe and Zn are 3.32 and 2.41 wt%, respectively, and the atomic ratio of Zn has increased to 0.47%, this phenomenon demonstrated that $ZnCl_2$ possesses the ability to create pores for biochar samples. In addition, with the addition of zinc ions, the atomic ratio of iron ions decreased, but the content was higher than that of unloaded samples, indicating that the two elements are successfully loaded at the same time and there is a certain competitive relationship between the two metal cations. In general, the morphological structure and EDS energy spectrum analysis show that iron and zinc are successfully loaded on the surface of BC.

The crystal structure of as-prepared BC, BC-Fe-1 and BC-Fe-1-Zn samples was investigated by XRD patterns. As presented in Fig. 2A, in the BC-Fe-1 sample, the strong peaks at 2θ= 35.48°, 43.10° and 62.77° corresponding to the diffraction peaks of γ-Fe_2O_3, indicating that the iron element is successfully loaded on the surface of BC. In addition, the surface magnetic γ-Fe_2O_3 particle is not only conducive to the recovery and secondary utilization of the catalyst, but also can effectively inhibit the leaching of metal ions [34]. To further verify the ferromagnetism of the prepared catalysts, the magnetic properties are measured with a vibrating sample magnetometer (VSM). Fig. S2 showed that BC-Fe-1-Zn possessed the characteristic of ferromagnetism [35], suggesting magnetic characteristics suitable for application in magnetic separation from aqueous solutions [36]. In addition, there is no obvious hysteresis in the magnetization curve of BC-Fe-1-Zn, which indicates that the remanence and coercivity of BC-Fe-1-Zn are zero. To sum up, BC-Fe-1-Zn is easy to recover and can avoid secondary pollution to the environment. As for BC-Fe-1-Zn sample, the strong peaks at 2θ = 31.81°, 34.62°, 36.41°,

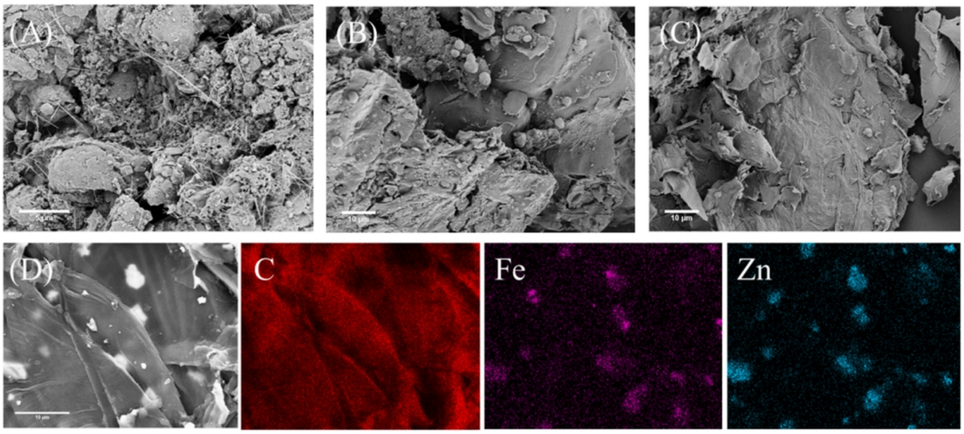

Fig. 1. The SEM images of (A) BC, (B) BC-Fe-1, (C) BC-Fe-1-Zn and (D) EDX images of BC-Fe-1-Zn samples.

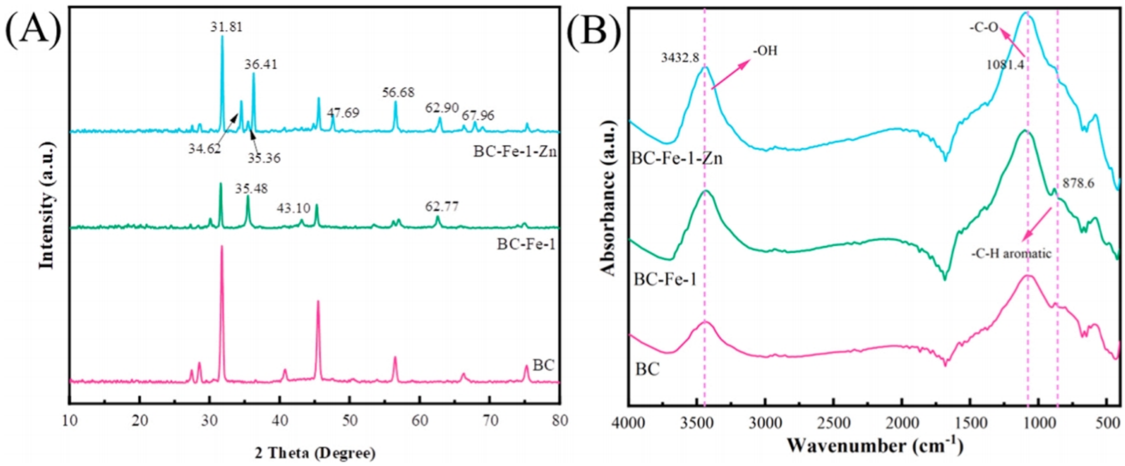

Fig. 2. (A) XRD patterns and (B) FTIR spectra of BC, BC-Fe-1 and BC-Fe-1-Zn samples.

47.69°, 56.68°, 62.90° and 67.96° represent the (100), (002), (101), (102), (110), (103) and (112) planes of the reflective surfaces of hexagonal wurtzite type ZnO (JCPDS, no. 00-003-0888). Moreover, there are more obvious characteristic peaks at $2\theta = 35.36°$ and 62.90°, which are attributed to characteristic diffraction peak of γ-Fe_2O_3 species [37]. After the addition of zinc, the characteristic peak of iron is significantly weakened, but it still coexists in the identical sample, which is consistent with the EDS results. These above results reflect that the iron and zinc elements are successfully attached to the BC, that is, the modification of BC is appropriate.

In this study, the specific surface area, pore volume and pore size of BC, BC-Fe-1 and BC-Fe-1-Zn samples were measured by the N_2 adsorption-desorption method. The characterization results are shown in Table S1, it can be obtained from the table that the specific surface area of BC-Fe-1 loaded with iron has increased from 123.33 $m^2\ g^{-1}$ to 160.22 $m^2\ g^{-1}$ with the pore volume increased from 5.24×10^{-3} to $6.30 \times 10^{-3}\ cm^3\ g^{-1}$ compared with BC alone. In this process, the pore size decreased severely. After loading zinc, the specific surface area of the BC-Fe-1-Zn material has been greatly increased, as high as 242.54 $m^2\ g^{-1}$ and the pore volume reached $8.20 \times 10^{-3}\ cm^3\ g^{-1}$, at the same time, the pore size has been reduced to 2.97 nm. During the whole material compounding process, the specific surface area and pore volume are increasing while the pore size is decreasing, which indicates that the addition of iron and zinc has a certain pore-forming effect on the peanut hull-derived biochar. A large specific surface area can expose more active sites which exhibits a positive role in promoting the activation reaction [38,39]. Consequently, the loading of transition metal iron and zinc on BC samples are of great significance in the enhanced catalytic degradation of TC.

Except for the change of morphology and crystal structure, in the process of BC-Fe-1-Zn synthesis, the chemical state and composition of the samples should be further investigated in detail. Therefore, the FTIR spectroscopy and XPS analysis were performed. The FTIR spectroscopy of BC, BC-Fe-1 and BC-Fe-1-Zn samples are shown in Fig. 2B, these three materials have multiple characteristic peaks. Among them, the characteristic peak at 3432.8 cm^{-1} is related to the hydrogen-oxygen bond (–OH), and the absorption peak around 1081.4 cm^{-1} is attributed to the stretching vibration modes of –CO groups [40], while the weak characteristic peak at 878.6 cm^{-1} is corresponding to the aromatic hydrocarbon –CH stretching vibration modes [41]. In addition, the peaks in the region 400–800 cm^{-1} referred to the metal elements vibration modes. Although the characteristic peak positions of the three samples are similar, they have different intensities and a certain degree of migration. From BC and BC-Fe-1 to BC-Fe-1-Zn composite samples, the characteristic peaks at 3432.8 cm^{-1} and 1081.4 cm^{-1} gradually increase. The characteristic peak at 878.6 cm^{-1} is relatively stable, and there is no obvious change, while the metal peaks between 800 cm^{-1} and 400 cm^{-1} have little increase. The changes of these absorption peaks indicate that the compounding of the materials enhances the catalytic performance of the composite samples.

The XPS analysis was executed to further investigate the chemical state and composition changes of these samples after the metals loaded on BC. In addition to analyzing the full-spectrum characteristics of these materials, the valence state changes of the two elements C and Fe are also investigated. The analogous XPS survey spectrum (Fig. S3) demonstrated that the elemental composition of samples mainly containing C, O and Zn elements. Due to the low content of Fe, so there is no obvious characteristic peak, however, Fe 2p spectra illustrating the successful loading of Fe on the surface of BC, which consistent with EDS elemental analysis results and previous research. In terms of C 1s high-resolution spectra in Fig. 3A–C, there were two particularly distinct component peaks and a relatively weak peak at 284.8 eV, 286.1 eV, and 288.7 eV, which represent the C—C, C—O and C═O bonds respectively [42]. With the addition of Fe element, the peak intensity of C–C and C═O both increase while that of C–O decreases. However, after adding Zn on the basis of BC-Fe-1 sample, the content of C–C and C═O decreased, and the content of C–O increased greatly. Interestingly, no electron peak of iron carbide has been found in the composite material, indicating that Fe does not directly react with biochar to bond together [43].

Furthermore, the Fe 2p spectra of these three samples in Fig. 3D–E revealed the two primary peaks at 712 eV and 724.9 eV, which could be allocated to the representative binding energy of Fe ions corresponding to Fe $2p_{3/2}$ and Fe $2p_{1/2}$, respectively. Specifically, the peaks at 709.72 eV and 712.14 eV in BC-Fe-1-Zn sample are attributed to Fe(II) and Fe(III) species, respectively [35], indicating the presence of Fe_2O_3 species in composites [44], the above results are consistent with the previous analysis of XRD patterns. In addition, the positions of binding energy of these two characteristic peaks are both about 5 eV lower than the corresponding satellite peaks. The formation of Fe_2O_3 may be as follows (Eqs. (1)–(3)):

$$Fe(NO_3)_3 + 3H_2O \rightarrow Fe(OH)_3 + 3HNO_3 \quad (1)$$

$$Fe(OH)_3 \rightarrow FeO(OH) + H_2O \quad (2)$$

$$2FeO(OH) \rightarrow Fe_2O_3 + H_2O \quad (3)$$

3.2. *Performance evaluation on PDS activation*

The efficiency of tetracycline (TC) degradation of pristine BC, PDS and BC/PDS system was first evaluated in continuously stirred solution at room temperature. As shown in Fig. 4A, in the adsorption system, the

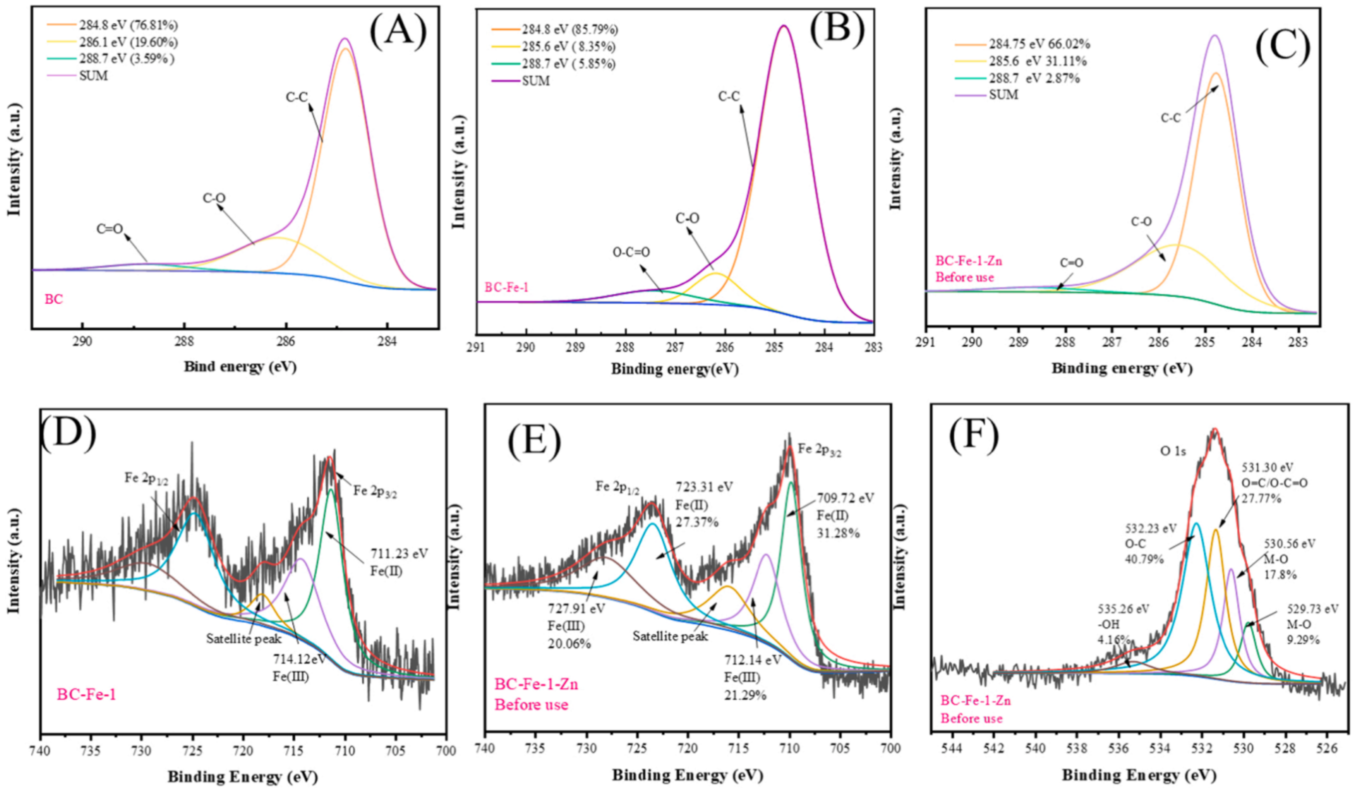

Fig. 3. XPS spectra of BC, BC-Fe-1 and BC-Fe-1-Zn samples: (A), (B) and (C) C 1s, (D-E) Fe 2p, (F) O 1s.

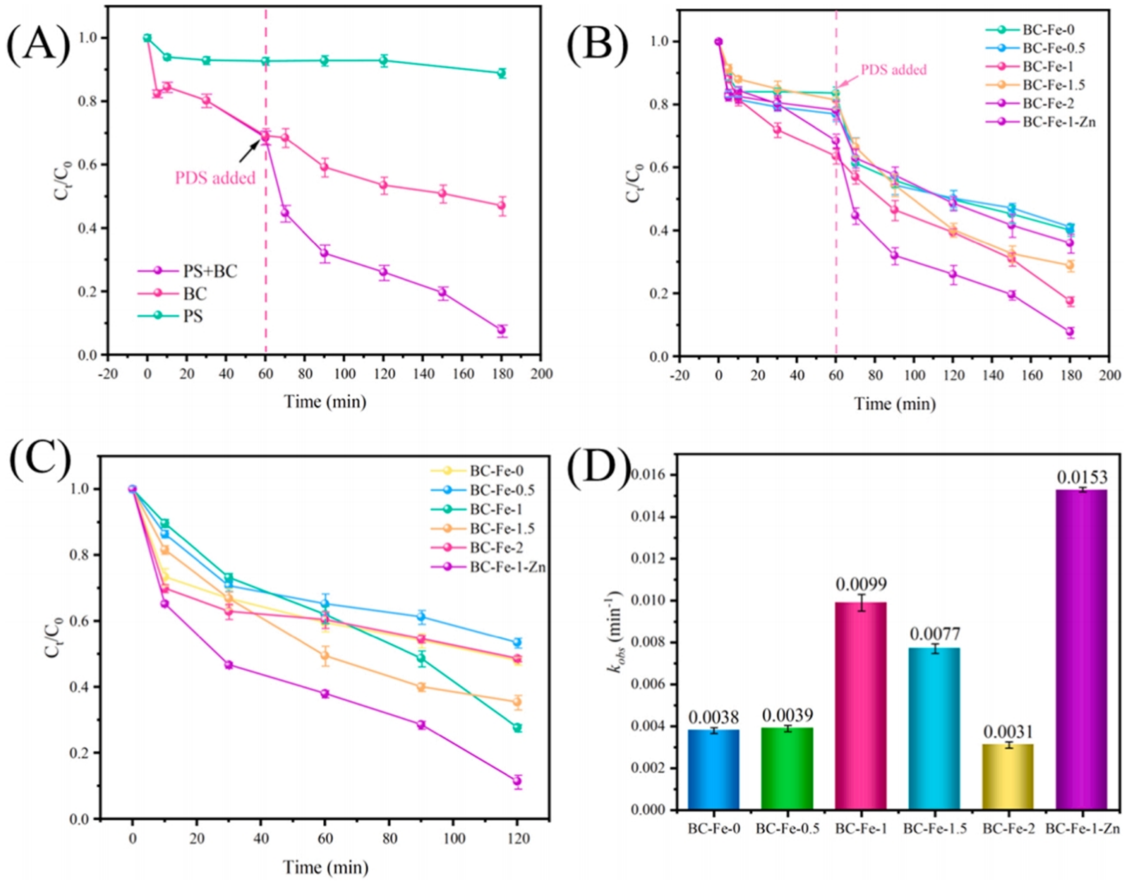

Fig. 4. (A) The degradation process of TC in PS, BC, and PS+BC systems. (B) The adsorption and degradation and (C) direct degradation of TC over BC-Fe-x and BC-Fe-1-Zn samples. (D) The kinetics constants of direct TC degradation. Experimental conditions: [PDS] = 2 g L^{-1}, [Catalysts] = 1 g L^{-1}, [TC] = 20 mg L^{-1}, pH = 3.

removal efficiency of PS to TC is about 10% within 180 min and that of BC is about 50%, indicating that the removal efficiency of TC by single PDS is very low and almost no effect on the degradation of TC. In addition, it also shows a certain adsorption capacity of BC to TC, however, it cannot effectively adsorb TC in wastewater. The TC can be effectively removed only when PDS and BC coexist at the same time. After the reaction of 180 min, the removal efficiency reached 92%. This is because PDS is activated by biochar and produce ROS, which generate oxidative reaction with pollutants to degrade them effectively. Subsequently, we further studied the degradation of TC when the oxidant PDS and modified biochar were coexisted and the results were shown in Fig. 4B. In order to verify that the addition of PDS can accelerate the degradation process, PDS is not added to the reaction system in the first 60 min. As can be seen from the figure, the degradation efficiency of biochar materials for TC is relatively low in the absence of PDS. The degradation effect of bulk BC is less than 20%, and that of composite material changes with the proportion. The removal efficiency of BC-Fe-1 is the highest, which reaches nearly 40%. After reaction for 60 min, the addition of PS accelerates the degradation of TC. The degradation efficiency of BC-Fe-1-Zn is the highest, which can reach more than 90% (180 min). Moreover, we have compared the experimental results of other BCs-based catalysts to activate persulfate to degrade tetracycline, and the results are shown in Table S2, from which we can find that the BC catalyst in this work still possess prominent and competitive tetracycline degradation efficiency.

A comparative experiment is set up to directly activate persulfate for TC degradation and the experimental results are shown in Fig. 4C. Before being modified, the removal efficiency of TC within 120 min is only about 50%. After Fe ions loaded, the degradation effect of TC by the composite samples firstly increased and then decreased with the change of proportion. Among them, the results show that, the BC-Fe-1 composite (biomass: $Fe(NO_3)_3 = 5:1$) exhibits enhanced removal effect on TC, which can remove 72% of TC in 120 min. Besides, in order to further improve the degradation efficiency of BC-Fe-1 composite, $ZnCl_2$ is introduced in the preparation process because of its pore-forming ability on biochar. The results illustrate that the addition of $ZnCl_2$ significantly improved the removal efficiency, which increases from 72% to 90%, indicating that BC-Fe-1-Zn (biomass: $Fe(NO_3)_3$: $ZnCl_2 = 5:1:1$) composite material can be used as an excellent catalyst for activation of PDS, and then generate reactive oxygen species to remove TC from water.

In order to better understand the degradation rate of TC under different samples, the pseudo-first order kinetic model (Eq. (4)) was applied to evaluate degradation rate constant over these catalysts [45]. By means of fitting the data in Fig. 4C into Eq. (4), the values of rate constant k can be reasonably estimated, and the results are shown in Fig. 4D.

$$ln\left(\frac{C_t}{C_0}\right) = -kt \tag{4}$$

Where C_0 and C_t are the concentrations of TC under preliminary conditions and at time t, respectively, k is the rate constant of first order. As shown in Fig. 4D, the degradation rate constants of TC by BC-Fe-0, BC-Fe-0.5, BC-Fe-1, BC-Fe-1.5, BC-Fe-2 and BC-Fe-1-Zn are 0.0038, 0.039, 0.0099, 0.0077, 0.0031 and 0.0153 min^{-1}, respectively. Such a 4.03-fold improvement of k value demonstrated the distinctly enhanced TC degradation efficiency of BC-Fe-1-Zn sample. Compared with BC and BC-Fe-1 catalysts, the outstanding performance of BC-Fe-1-Zn may be ascribed to the uniform distribution of Fe and Zn on biochar and the synergistic effect between them. On the other hand, the increased specific surface area is conducive to exposing more active sites, thus enhancing the interaction among pollutants, PDS and catalysts.

Due to the composition of the actual sewage is complicated and changeable, it is necessary to investigate some actual factors that may affect the catalytic efficiency of this system. Therefore, the effects of pH, anions, catalyst concentration and PDS dosage on the degradation efficiency of TC are investigated. The removal effect of BC-Fe-1-Zn activated PS to degrade TC under different pH conditions as depicted in Fig. S4A. With the change of pH value, the degradation trend of TC is roughly the same, but it obviously shows different degradation efficiency, which indicates that the BC-Fe-1-Zn sample can be applied to a wide pH range. The experimental results show that the BC-Fe-1-Zn/PDS system has good adaptability within the initial pH adjustment range. It can be seen from the figure that the degradation of TC by BC-Fe-1-Zn only maintains a high efficiency in the first 30 min under different pH value. With the progress of the reaction, the degradation efficiency decreases gradually, this may be due to the large amount of active substances consumed during the process. In addition, as the pH of the system environment decreases, the degradation effect becomes better. When the pH value is 3 and 5, the degradation curve of TC has an obvious downward trend, and the ultimate rate constants k under the pH condition are 0.0167 min^{-1} and 0.0153 min^{-1} (Fig. S4B), respectively. As the pH value increases, the reaction rate constant becomes smaller, which shows that acidic condition is more conducive to the degradation of TC. This may be because different pH conditions will affect the state of BC-Fe-1-Zn, PDS and TC in aqueous solution [17]. Further combining the Zeta potential of different composite materials to study the effect of pH, the electromotive potential values of catalysts are shown in Fig. S4C in which we can see that under this reaction condition, the potential of each material is negative. It shows that the surface of these materials is negatively charged under this system. When $pH < 4$, the surface of TC is positively charged [46], which is more conducive to the reaction of these composite materials with TC. Moreover, the Zeta potential of BC is the largest without any element doping, that is, the ability to react with positively charged pollutants is weaker. With the addition of Fe and Zn, the potential value of the composite material shows a trend that first decreases, then rises, and finally stabilizes. The potential value of the BC-Fe-1-Zn composite material is the smallest (− 52.7 mV), which is consistent with the best reaction effect of the material. In addition, metal ions are more likely to migrate to the liquid phase under acidic conditions, which can activate PDS to generate more ROS and then provide more effective catalytic components.

To investigate the effect of anions on the overall catalytic efficiency, the anions of Cl^-, NO_3^- and SO_4^{2-} are introduced into the reaction system. As shown in Fig. S5A, the degradation rate of TC is basically the same in the first 10 min of reaction. As the reaction progresses, the degradation rate of TC is different under different conditions, but the difference is not significant when the reaction reaches the end point. Under different conditions, the first-order reaction constant k is between 0.0153 min^{-1} and 0.0144 min^{-1} (Fig. S5B). It can be explained that the existence of these anions basically exhibits no significant effect on the process of BC-Fe-1-Zn composite material activated PDS to generate free radicals to remove TC. Moreover, the catalyst and PDS concentration also have an impact on the efficiency of the entire catalytic system, and thus the discussion on this aspect is equally meaningful. As shown in Fig. S6A, when the concentration of BC-Fe-1-Zn is lower than 2 g L^{-1}, the adsorption and removal efficiency of TC is low (15–25%), which may be due to the low content of biochar. Only when the concentration of biochar reaches a certain value (1 g L^{-1}) will there be a better adsorption and removal effect. PDS is added to the reaction after 60 min, and the degradation rate of TC is greatly accelerated, and the dosage of BC-Fe-1-Zn is 1 g L^{-1} and 2 g L^{-1}, the removal efficiency is almost 100%, correspondingly, the reaction constants k are 0.0153 min^{-1} and 0.02231 min^{-1}, respectively (Fig. S6B). This is because as the catalyst concentration increases, more active sites will be introduced in catalytic system, thereby accelerating the degradation rate of TC. By the way, from the perspective of saving raw materials, the optimal dosage of BC-Fe-1-Zn is selected as 1 g L^{-1}.

The effect of BC-Fe-1-Zn on the removal of TC under different PDS dosages (0.5 g L^{-1}, 1 g L^{-1}, 2 g L^{-1} and 3 g L^{-1}) is displayed in Fig. S7A. The results show that when the PDS concentration is 0.5–3 g L^{-1}, the degradation rate of TC in the first 60 min is consistent, and the removal efficiency of TC reaches 68.56%. After 60 min, the degradation rates of TC under different PDS concentrations are different, when the PDS concentration is 0.5 g L^{-1}, the degradation efficiency of TC is the lowest. The degradation rate of TC increases with the increase of PDS dosage, and when the PDS concentration is 3 g L^{-1}, the k value is the largest (0.0177 min^{-1}). In addition, the k value of PDS concentration increases the most in the interval of 1 g L^{-1} and 2 g L^{-1}, reaching 0.0044 min^{-1} (Fig. S7B), which indicates that the degradation rate of TC does not increase uniformly with the increase of PDS concentration. It may be that the ROS generated insufficiently when the PDS concentration at low levels, so the degradation rate of TC increases slowly. When the PDS concentration reaches a certain high level, more ROS can be generated to achieve a relatively stable degradation effect. When the PDS concentration is 2 g L^{-1} and 3 g L^{-1}, the degradation efficiency of TC is almost 100% (180 min), and therefore the optimal dosage of PDS in this study is 2 g L^{-1}.

3.3. Identification of reactive oxygen species and reaction mechanisms

The degradation pathways of the PDS activation system to pollutants are mainly divided into two types: free radical pathways ($SO_4^{\bullet-}$, $^{\bullet}OH$ and $O_2^{\bullet-}$) and non-radical pathways (direct electron transfer pathway and $^1O_2$). Among them, the types of these free radicals can be verified by trapping experiments due to the trapping agent have an inhibitory effect on the reaction of ROS and can indirectly reflect the role of free radicals. In order to investigate which ROS is at work under this catalytic system, some quenching experiments are carried out. Ethyl alcohol (EtOH) and tert-butanol (TBA) are selected as ROS quenching agents in this experiment. The kinetic constants of EtOH react with $SO_4^{\bullet-}$ and $^{\bullet}OH$ are $1.6–7.8 \times 10^7$ M^{-1} s^{-1} and $1.2–2.8 \times 10^9$ M^{-1} s^{-1}, respectively [47], which shows that it has high reactivity to these two kinds of free radicals. The reaction rate of TBA with $^{\bullet}OH$ is $3.8–7.6 \times 10^8$ M^{-1} s^{-1}, which is about 1000 times higher than that with $SO_4^{\bullet-}$ ($4–9.1 \times 10^5$ M^{-1} s^{-1}) [48], so TBA is more inclined to react with $^{\bullet}OH$ under this condition. In addition, in order to explore whether the system has the effect of $O_2^{\bullet-}$, a quenching experiment is conducted with benzoquinone (BQ) as a trapping agent with a rapid react rate ($k(O_2^{\bullet-}) = 1 \times 10^9$ M^{-1} s^{-1}) [47]. As shown in Fig. 5A, the degradation efficiency of TC is severely inhibited after adding EtOH and TBA, and reduced to 41.04% and 51.17% within 120 min, respectively. However, the removal effect almost not restrained in the presence of BQ trapping agent in previous 100 min, which still reaches 80% in 120 min. The above results indicates that the TC degradation mainly follows the radical pathway, of where $SO_4^{\bullet-}$and $^{\bullet}OH$ are the dominant active species, and the influence of $O_2^{\bullet-}$ is negligible. Correspondingly, the reaction kinetic constant k also reflects this inference very well (Fig. 5B). The first-order reaction constant k of TC degradation reduced from 0.0153 to 0.0045 min^{-1} after the addition of EtOH. Similarly, the inhibitory effect of TBA is also obvious and k is reduced to 0.0056 min^{-1}, the results show that $SO_4^{\bullet-}$ and $^{\bullet}OH$ are the main types of active substances in the catalytic system.

In order to explore the active species in the reaction more comprehensively, the possible non-radical pathway active substance is investigated. Therefore, the sodium azide (NaN_3) is served as the quencher for $^1O_2$ with a reaction rate of 1×10^9 M^{-1} s^{-1} in the capture experiment [49]. As depicted in Fig. 5A, the TC degradation of the BC-Fe-1-Zn/PDS system is slightly inhibited, and the degradation efficiency of TC can still reach 79.96% with reaction rate constant of 0.0116 min^{-1} after adding trapping agent NaN_3 (Fig. 5B). This phenomenon demonstrates that $^1O_2$ almost not involved in the catalytic degradation reaction, and it is unrealistic to degrade pollutants through non-radical pathways in such a system.

To prove the existence of these reactive species in the process of TC

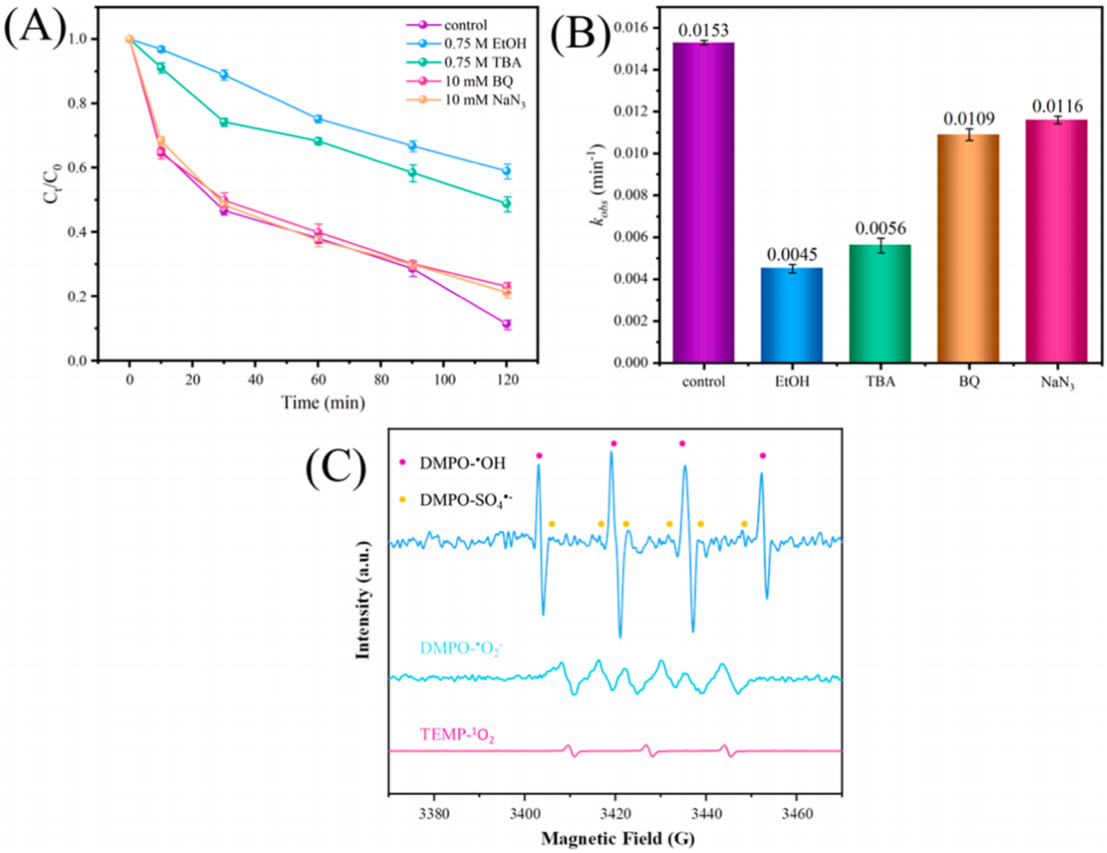

Fig. 5. (A) Influence of different quenching agents in PDS+BC-Fe-1-Zn systems. (B) The kinetics constants of TC degradation with different quenching agents. Experimental conditions: [PDS] = 2 g L^{-1}, [Catalysts] = 1 g L^{-1}, [TC] = 20 mg L^{-1}, pH = 3. (C) EPR spectra recorded in DMPO/TEMP + PDS + BC-Fe-1-Zn systems.

degradation, the EPR spectra characterization of DMPO-$SO_4^{\bullet-}$, DMPO-$^{\bullet}$OH, DMPO-$\bullet O_2^-$ and TEMP-$^1O_2$ were performed over BC-Fe-1-Zn/PS system. As displayed in Fig. 5C, a four-line EPR signal with an intensity ratio of 1:2:2:1 was clearly observed at 10 min after the addition of PS, which was attributed to DMPO-$^{\bullet}$OH, and the DMPO-$SO_4^{\bullet-}$signal exhibited six lines in 1:1:1:1:1:1. No obvious signal of $^1O_2$ could be obtained when BC-Fe-1-Zn was added, and the EPR signal of DMPO-$\bullet O_2^-$ in this system was very weak indicated that its content was low, in addition, the oxidizing power of $\bullet O_2^-$ was inferior to that of $SO_4^{\bullet-}$ and $^{\bullet}$OH. This result further confirmed the conclusion of the quenching experiment.

3.4. *Catalytic mechanisms in BC-Fe-1-Zn/PS system*

The reactive sites and the activation mechanism of PS can be further illustrated by the XPS spectra of the used BC-Fe1-Zn catalyst (Fig. 6). After the reaction, the Fe(III) content increased from 41.35% to 46.94% and the Fe(II) decreased from 58.65% to 53.06% (Fig. 6A). This indicated that Fe(II) can promote the activation of PDS, in general, Fe(III) must be reduced into Fe(II) firstly to participate in the reaction rather than directly generate $SO_4^{\bullet-}$ by reacting with PDS in such a AOP system. The Fe(III) reduction in this system might be achieved by reacting with PDS (Eq. (5)), then the generated Fe(II) with higher catalytic activity could transfer electrons to PDS to produce $SO_4^{\bullet-}$ (Eq. (6)), further, $SO_4^{\bullet-}$ can be converted into $\bullet$OH by water consumption (Eq. (7)) [50]. The changes in the content before and after the reaction proved this mechanism.

$$\mathrm{Fe(III)} + S_2O_8{}^{2-} \rightarrow \mathrm{Fe(II)} + S_2O_8{}^{\bullet-} \tag{5}$$

$$\mathrm{Fe(II)} + S_2O_8{}^{2-} \rightarrow \mathrm{Fe(III)} + SO_4^{\bullet-} + SO_4^{2-} \tag{6}$$

$$SO_4^{\bullet-} + H_2O \rightarrow SO_4^{2-} + \bullet OH + H+ \tag{7}$$

Furthermore, there were obvious content variation of C 1s spectra of the used BC-Fe-1-Zn catalyst (Fig. 6B). The three peaks at 284.7, 285.35, 287.65 eV are corresponding to C-C, C-O and C=O groups, respectively. The relative content of C-O of BC-Fe-1-Zn reduced from 31.11% to 26.38% after reaction. It has been illustrated that oxygen-containing functional groups on the surface of catalysts could affect their catalytic properties [35]. The corresponding O 1s spectra of used catalyst were shown in Fig. 6C, the contents of -OH and O-C of the used BC-Fe-1-Zn reduced from 4.16% and 40.79–0% and 31.63%, respectively, while the contents of M-O (M: Fe or Zn) groups increased from 27.09% to 28.75%. The above results indicated that both –OH, C–O and M−O were the main catalytic sites for activating PDS in this system.

The electrochemical characteristic is regarded as an efficacious accordance for assessing the current responses and the electrons transfer of the catalytic system [51]. Fig. 7A illustrated the EIS of the bare glassy carbon electrode (GCE) and BC-Fe-1-Zn sample by depositing the obtained samples on a FTO substrate. As we know, the diameter of the first semicircles of the EIS curves represented the electron transfer resistance, and the BC-Fe-1-Zn sample possessed smaller arc radius than that of the bare GCE, indicating a smaller carrier transfer resistance, which possess a positive promotion to the charge transfer. The current intensity responses of different systems are shown in Fig. 7B, when GCE coexists with PS and TC, there is almost no current. The current begins to change with the addition of BC-Fe-1-Zn composite material, and the current value is the highest when BC-Fe-1-Zn, PS and TC coexist. The electrochemical characterizations show that the existence of electron transfer promotes the rapid generation of active free radicals in the efficient degradation of TC.

Through the identification and investigation of reactive oxidizing species as well as the previous characterization analysis, we have a clear understanding of the reaction mechanisms of BC-Fe-1-Zn material activated PDS to catalyze the degradation of TC. The enhanced catalytic performance of BC-Fe-1-Zn can be attributed to the following aspects. Firstly, the specific surface area and pore volume of the BC-Fe-1-Zn are increased in the process of precursor reaction, and the introduction of Zn on the surface of BC-Fe-1 greatly reduced the pore diameter (from 11.07 nm to 2.97 nm). The increased specific surface area can provide more active sites for catalytic reactions and at the same time increase the accessibility of pollutants, PDS and catalysts, greatly improving the reaction kinetics of the system. Secondly, the successful decoration of inherent Fe and Zn elements on the surface of BC not only changes the morphology of the material, but also improves the physicochemical properties. FTIR and XPS characterizations show that the composite BC-Fe-1-Zn material has more –CO, –CH, –OH functional groups, and which may participate in the activation process of PDS (Eqs. (8)–(9)) [52]. In addition, the content of C–C and C=O decreased before and after compounding while the content of C–O increased. It is possible that C–O plays a greater role in the degradation of TC, which was consistent with previous research results [53]. On the other hand, the Zeta potential of the catalyst has changed obviously and the potential of BC-Fe-1-Zn sample is the lowest, which makes it easier to adsorb positively charged pollutants and this is consistent with the best degradation effect under this system. Finally, the Fe and Zn atoms in the catalysts can accelerate electrons transfer between pollutants and PDS, and then PDS is reduced to generate free radicals and other reactive oxygen species with strong oxidizing properties to degrade pollutants (Eqs. (10)–(13)) [37,54]. The biochar matrix also served as an excellent electron transfer support to facilitate the activation of PDS via oxidizing the absorbed water to produce $^{\bullet}$OH. Furthermore, biochar matrix could protect Fe and Zn from leaching and transfer electrons to Fe(III) directly to accelerate Fe(III)/Fe(II) cycle, which is favorable for the decomposition of PDS. Consequently, the synergistic effect between biochar and Fe and Zn species is of positive significance for enhancing the performance of the catalytic system. Based on abovementioned analysis, the reaction mechanisms in this system can be illustrated in Fig. 8. The specific

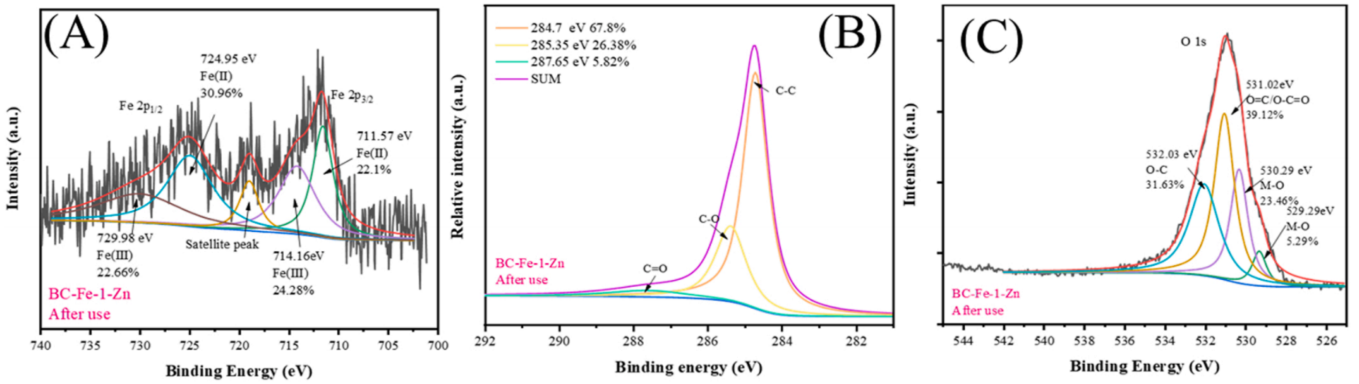

Fig. 6. The XPS spectra of Fe 2p, C 1s and O 1s of the used BC-Fe-1-Zn catalyst.

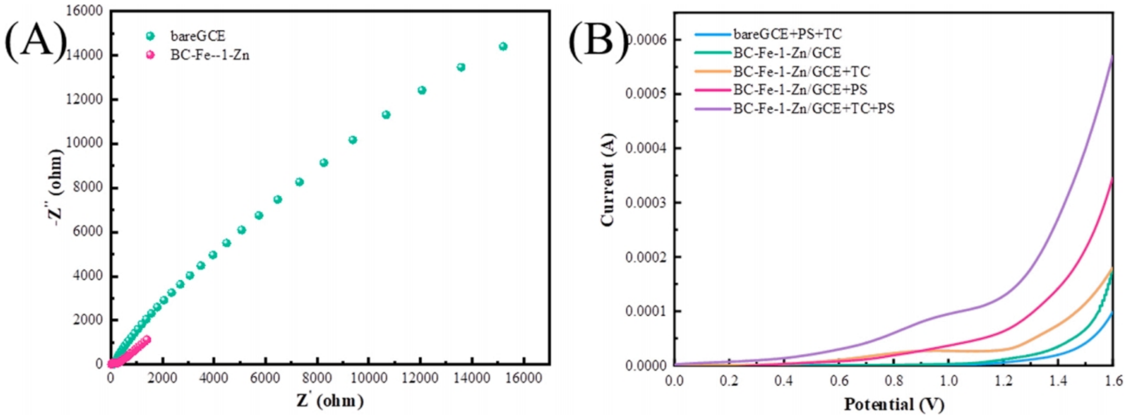

Fig. 7. (A) The Nyquist plots (EIS) of GCE and GCE loaded with BC-Fe-1-Zn sample. (B) LSV of GCE and GCE loaded with BC-Fe-1-Zn under different reaction conditions. Experimental conditions: [PDS] = 2 g L^{-1}, [Catalysts] = 1 g L^{-1}, [TC] = 20 mg L^{-1}.

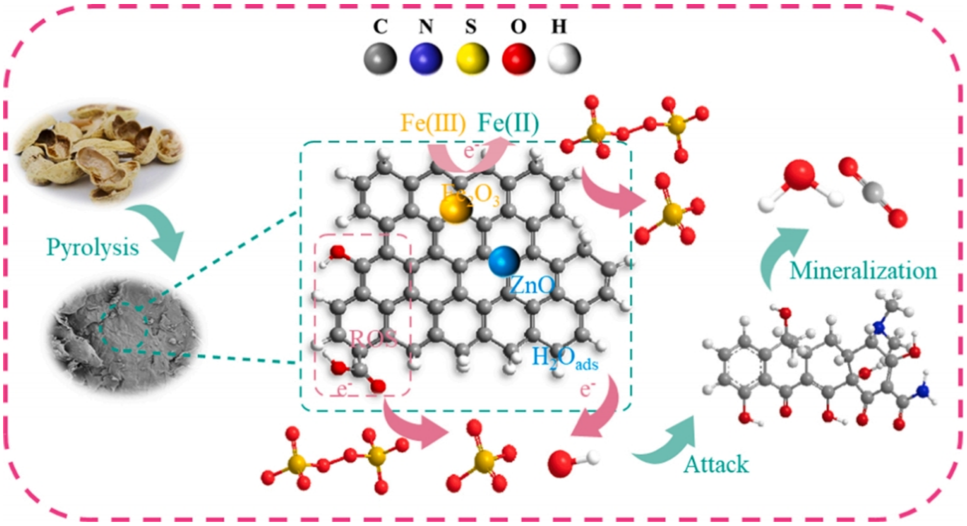

Fig. 8. Proposed mechanism of persulfate activated by BC-Fe-1-Zn catalyst for enhanced tetracycline degradation.

reaction processes are shown in the following formulas:

$$BC_{surface}–OOH + S_2O_8{}^{2-} \rightarrow SO_4^{\bullet -} + BC_{surface}\text{-}OO\bullet + HSO_4^- \tag{8}$$

$$BC_{surface}–OH + S_2O_8{}^{2-} \rightarrow SO_4^{\bullet -} + BC_{surface}–O\bullet + HSO_4^- \tag{9}$$

$$S_2O_8{}^{2-} + e^- \rightarrow SO_4^{\bullet -} + SO_4^{2-} \tag{10}$$

$$S_2O_8{}^{2-} + H_2O \rightarrow HO_2^- + 2SO_4^- + H^+ \tag{11}$$

$$S_2O_8{}^{2-} + HO_2^- \rightarrow SO_4^{2-} + SO_4^{\bullet -} + O_2^{\bullet -} + H^+ \tag{12}$$

$$SO_4^{\bullet -} + OH^- \rightarrow SO_4^{2-} + \bullet OH \tag{13}$$

3.5. *Possible degradation pathway of TC*

To illustrate the produced degradation intermediates of TC in BC-Fe-1-Zn/PS system, HPLC-MS was employed and the degradation process at the optimal conditions was chosen to be investigated. As proved in previous analysis, all intermediates produced from the attack of $SO_4^{\bullet -}$ and $^\bullet OH$. In general, $^\bullet OH$ is inclined to addition reactions or hydrogen abstraction, while $SO_4^{\bullet -}$ is more involved in electron transfer process reactions. Therefore, based on the results of the HPLC-MS spectra in Fig. S8, the possible three degradation pathways of TC by BC-Fe-1-Zn/PS were proposed in Fig. 9. As for pathway I, it mainly included dealkylation and dehydration processes. The TC was subjected to a dehydration and N-methyl group removal reaction to form P1 (*m/z* 400) firstly. Then, the acylamino group in P1 was attacked by $SO_4^{\bullet -}$ and $^\bullet OH$ to form the P2 (*m/z* 362). At the same time, due to the presence of strong oxidizing $^\bullet OH$, the carbocyclic ring in P2 could be directly cleaved to form P3 (*m/z* 318). Afterwards, P3 could be further oxidized to the intermediate P4 (*m/z* 274) [55]. In the pathway II, it mainly included the addition reaction of C═C bond and dehydration reaction [6]. The C═C bond in aromatic ring of TC was attacked by $^\bullet OH$ to form an intermediate P5 (*m/z* 461) firstly. Next, $SO_4^{\bullet -}$ was continuously attacked P5 to obtain the intermediate product P6 (*m/z* 477). In the pathway III, P7 (417 *m/z*) was formed by demethylation of TC. Then, P8 (385 *m/z*) and P9 (353 *m/z*) were generated by demethylation and hydrogen abstraction with the help of the oxidative capability of $^\bullet OH$ [35]. Ultimately, as the catalytic reaction proceeds, the above intermediates continued to be degraded into small molecules until mineralization into CO_2 and H_2O.

4. Conclusions

In summary, we propose a novel catalyst for persulfate activation, viz., BC-1-Fe-Zn composite, which is prepared over peanut hull-derived biochar with foreign Fe and Zn loading. The composite catalysts can effectively active PDS for the degradation of TC pollutants through free radical pathways with $SO_4^{\bullet -}$ and $^\bullet OH$ play a key role in this system. A

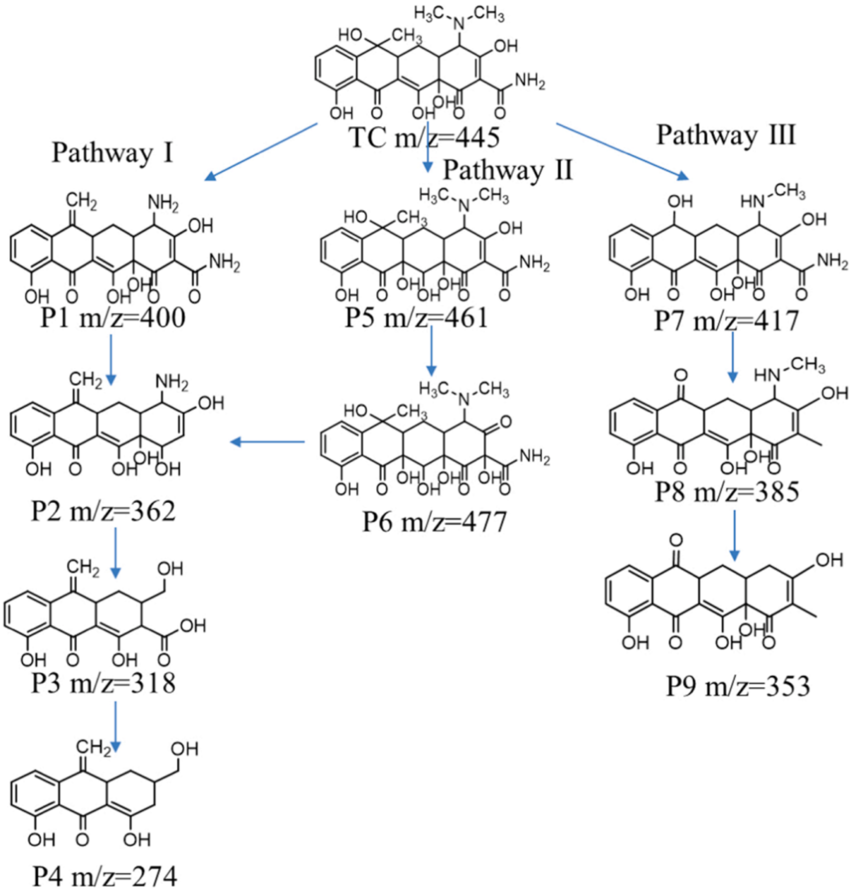

Fig. 9. Proposed degradation process of TC.

series of experiments and characterizations find that the enhanced catalytic activity is mainly due to the increase in specific surface area, the effect of surface functional groups and the rapid electron transfer process, which can accelerate the generation of free radicals and quickly catalyze the degradation of pollutants. pH (3–11) and anions (SO_4^{2-}, Cl^- and NO_3^-) have no obvious effect on the degradation of TC, indicating that BC-1-Fe-Zn possesses an outstanding practical application potential. The developed BC-1-Fe-Zn/PDS method provides a promising strategy for a cost-effective mass production of catalyst for persulfate activation and their subsequent application in AOP wastewater treatment at the industrial scale.

CRediT authorship contribution statement

Yuan Pan: Conceptualization, Methodology, Investigation, Validation, Writing – original draft. **Zan Peng:** Conceptualization, Methodology, Investigation, Writing – original draft. **Zhifeng Liu:** Conceptualization, Resources, Project administration, Funding acquisition. **Binbin Shao:** Validation, Writing – review & editing. **Qinghua Liang:** Validation, Writing – review & editing. **Qingyun He:** Investigation, Data curation. **Ting Wu:** Investigation, Data curation. **Xiansheng Zhang:** Data curation. **Chenhui Zhao:** Investigation, Data curation. **Yang Liu:** Validation, Writing – review & editing. **Lin Ge:** Writing – review & editing. **Miao He:** Writing – review & editing.

Declaration of Competing Interest

The authors declare that they have no known competing financial interests or personal relationships that could have appeared to influence the work reported in this paper.

Acknowledgements

The study was financially supported by the Program for Changjiang Scholars and Innovative Research Team in University (IRT-13R17), the National Natural Science Foundation of China (52100181, 51979103, 51909085, 51679085, 51579096, 51521006, 51508177), the Fundamental Research Funds for the Central Universities of China (531107051205), the Funds of Hunan Science and Technology Innovation Project (2018RS3115, 2020RC5012), the Key Research and Development Project of Hunan Province of China (2017SK2241), Natural Science Foundation of Hunan Province, China (2020JJ5069), Funded by China Postdoctoral Science Foundation (2021T140192, 2021M690054).

Appendix A. Supporting information

Supplementary data associated with this article can be found in the online version at doi:10.1016/j.jece.2022.107366.

References

[1] Q. Liang, X. Liu, B. Shao, L. Tang, Z. Liu, W. Zhang, S. Gong, Y. Liu, Q. He, T. Wu, Y. Pan, S. Tong, Construction of fish-scale tubular carbon nitride-based heterojunction with boosting charge separation in photocatalytic tetracycline degradation and H_2O_2 production, Chem. Eng. J. 426 (2021), 130831.

[2] Q. Liang, X. Liu, G. Zeng, Z. Liu, L. Tang, B. Shao, Z. Zeng, W. Zhang, Y. Liu, M. Cheng, W. Tang, S. Gong, Surfactant-assisted synthesis of photocatalysts: mechanism, synthesis, recent advances and environmental application, Chem. Eng. J. 372 (2019) 429–451.

[3] Y. Pan, X. Liu, W. Zhang, Z. Liu, G. Zeng, B. Shao, Q. Liang, Q. He, X. Yuan, D. Huang, M. Chen, Advances in photocatalysis based on fullerene C_{60} and its derivatives: properties, mechanism, synthesis, and applications, Appl. Catal. B Environ. 265 (2020), 118579.

[4] B. Shao, X. Liu, Z. Liu, G. Zeng, Q. Liang, C. Liang, Y. Cheng, W. Zhang, Y. Liu, S. Gong, A novel double Z-scheme photocatalyst $Ag_3PO_4/Bi_2S_3/Bi_2O_3$ with enhanced visible-light photocatalytic performance for antibiotic degradation, Chem. Eng. J. 368 (2019) 730–745.

[5] B. Shao, Z. Liu, G. Zeng, Y. Liu, Q. Liang, Q. He, T. Wu, Y. Pan, J. Huang, Z. Peng, S. Luo, C. Liang, X. Liu, S. Tong, J. Liang, Synthesis of 2D/2D CoAl-LDHs/$Ti_3C_2T_x$ Schottky-junction with enhanced interfacial charge transfer and visible-light photocatalytic performance, Appl. Catal. B Environ. 286 (2021), 119867.

[6] Q. Liang, X. Liu, J. Wang, Y. Liu, Z. Liu, L. Tang, B. Shao, W. Zhang, S. Gong, M. Cheng, Q. He, C. Feng, In-situ self-assembly construction of hollow tubular g-C_3N_4 isotype heterojunction for enhanced visible-light photocatalysis: experiments and theories, J. Hazard. Mater. 401 (2021), 123355.

[7] Y. Liu, M. Cheng, Z. Liu, G. Zeng, H. Zhong, M. Chen, C. Zhou, W. Xiong, B. Shao, B. Song, Heterogeneous Fenton-like catalyst for treatment of rhamnolipid-solubilized hexadecane wastewater, Chemosphere 236 (2019), 124387.

[8] Y. Liu, Z. Liu, D. Huang, M. Cheng, G. Zeng, C. Lai, C. Zhang, C. Zhou, W. Wang, D. Jiang, H. Wang, B. Shao, Metal or metal-containing nanoparticle@MOF nanocomposites as a promising type of photocatalyst, Coord. Chem. Rev. 388 (2019) 63–78.

[9] B. Shao, X. Liu, Z. Liu, G. Zeng, W. Zhang, Q. Liang, Y. Liu, Q. He, X. Yuan, D. Wang, S. Luo, S. Gong, Synthesis and characterization of 2D/0D g-C_3N_4/CdS-nitrogen doped hollow carbon spheres (NHCs) composites with enhanced visible light photodegradation activity for antibiotic, Chem. Eng. J. 374 (2019) 479–493.

[10] B. Shao, Z. Liu, G. Zeng, Y. Liu, X. Yang, C. Zhou, M. Chen, Y. Liu, Y. Jiang, M. Yan, Immobilization of laccase on hollow mesoporous carbon nanospheres: noteworthy immobilization, excellent stability and efficacious for antibiotic contaminants removal, J. Hazard. Mater. 362 (2019) 318–326.

[11] B. Shao, J. Wang, Z. Liu, G. Zeng, L. Tang, Q. Liang, Q. He, T. Wu, Y. Liu, X. Yuan, Ti3C2Tx MXene decorated black phosphorus nanosheets with improved visible-light photocatalytic activity: experimental and theoretical studies, J. Mater. Chem. A 8 (2020) 5171–5185.

[12] B. Shao, Z. Liu, G. Zeng, H. Wang, Q. Liang, Q. He, M. Cheng, C. Zhou, L. Jiang, B. Song, Two-dimensional transition metal carbide and nitride (MXene) derived quantum dots (QDs): synthesis, properties, applications and prospects, J. Mater. Chem. A 8 (2020) 7508–7535.

[13] T. Wu, X. Liu, Y. Liu, M. Cheng, Z. Liu, G. Zeng, B. Shao, Q. Liang, W. Zhang, Q. He, W. Zhang, Application of QD-MOF composites for photocatalysis: energy production and environmental remediation, Coord. Chem. Rev. 403 (2020), 213097.

[14] T. Wu, Q. He, Z. Liu, B. Shao, Q. Liang, Y. Pan, J. Huang, Z. Peng, Y. Liu, C. Zhao, X. Yuan, L. Tang, S. Gong, Tube wall delamination engineering induces photogenerated carrier separation to achieve photocatalytic performance improvement of tubular g-C_3N_4, J. Hazard. Mater. (2021), 127177.

[15] J. Huang, X. Liu, W. Zhang, Z. Liu, H. Zhong, B. Shao, Q. Liang, Y. Liu, W. Zhang, Q. He, Functionalization of covalent organic frameworks by metal modification: construction, properties and applications, Chem. Eng. J. 404 (2021), 127136.

[16] Y. Hu, C. Zhou, H. Wang, M. Chen, G. Zeng, Z. Liu, Y. Liu, W. Wang, T. Wu, B. Shao, Q. Liang, Recent advance of graphene/semiconductor composite nanocatalysts: synthesis, mechanism, applications and perspectives, Chem. Eng. J. 414 (2021), 128795.

[17] S. Xiao, M. Cheng, H. Zhong, Z. Liu, Y. Liu, X. Yang, Q. Liang, Iron-mediated activation of persulfate and peroxymonosulfate in both homogeneous and heterogeneous ways: a review, Chem. Eng. J. 384 (2020), 123265.

[18] C. Zhao, B. Shao, M. Yan, Z. Liu, Q. Liang, Q. He, T. Wu, Y. Liu, Y. Pan, J. Huang, J. Wang, J. Liang, L. Tang, Activation of peroxymonosulfate by biochar-based catalysts and applications in the degradation of organic contaminants: a review, Chem. Eng. J. 416 (2021), 128829.

[19] J. Wang, S. Wang, Preparation, modification and environmental application of biochar: a review, J. Clean. Prod. 227 (2019) 1002–1022.

[20] S. Liu, W.-H. Xu, Y.-G. Liu, X.-F. Tan, G.-M. Zeng, X. Li, J. Liang, Z. Zhou, Z.-l Yan, X.-X. Cai, Facile synthesis of Cu(II) impregnated biochar with enhanced adsorption activity for the removal of doxycycline hydrochloride from water, Sci. Total Environ. 592 (2017) 546–553.

[21] Z. Peng, X. Liu, W. Zhang, Z. Zeng, Z. Liu, C. Zhang, Y. Liu, B. Shao, Q. Liang, W. Tang, X. Yuan, Advances in the application, toxicity and degradation of carbon nanomaterials in environment: a review, Environ. Int. 134 (2020), 105298.

[22] P. Godlewska, H.P. Schmidt, Y.S. Ok, P. Oleszczuk, Biochar for composting improvement and contaminants reduction. A review, Bioresour. Technol. 246 (2017) 193–202.

[23] S. Wang, J. Wang, Activation of peroxymonosulfate by sludge-derived biochar for the degradation of triclosan in water and wastewater, Chem. Eng. J. 356 (2019) 350–358.

[24] G. Fang, C. Liu, J. Gao, D.D. Dionysiou, D. Zhou, Manipulation of persistent free radicals in biochar to activate persulfate for contaminant degradation, Environ. Sci. Technol. 49 (2015) 5645–5653.

[25] J. Liang, X. Xu, W.Q. Zaman, X. Hu, L. Zhao, H. Qiu, X. Cao, Different mechanisms between biochar and activated carbon for the persulfate catalytic degradation of sulfamethoxazole: roles of radicals in solution or solid phase, Chem. Eng. J. 375 (2019), 121908.

[26] X. Wang, R. Deng, W. Shen, J. Huang, Q. Li, Y. Zhao, J. Wan, Y. Zhou, T. Long, S. Zhang, Rapid degradation of nitrochlorobenzene by activated persulfate oxidation with biochar supported nanoscaled zero valent iron, Front. Chem. 9 (2021).

[27] T. Yang, Y. Xu, Q. Huang, Y. Sun, X. Liang, L. Wang, X. Qin, L. Zhao, Adsorption characteristics and the removal mechanism of two novel Fe-Zn composite modified biochar for Cd(II) in water, Bioresour. Technol. 333 (2021), 125078.

[28] Y. Yu, Q. An, L. Jin, N. Luo, Z. Li, J. Jiang, Unraveling sorption of Cr (VI) from aqueous solution by $FeCl_3$ and $ZnCl_2$-modified corn stalks biochar: implicit mechanism and application, Bioresour. Technol. 297 (2020), 122466.

[29] H. Noei, H. Qiu, Y. Wang, E. Löffler, C. Wöll, M. Muhler, The identification of hydroxyl groups on ZnO nanoparticles by infrared spectroscopy, PCCP 10 (2008) 7092–7097.

[30] T. Yang, Y. Xu, Q. Huang, Y. Sun, X. Liang, L. Wang, X. Qin, L. Zhao, An efficient biochar synthesized by iron-zinc modified corn straw for simultaneously immobilization Cd in acidic and alkaline soils, Environ. Pollut. 291 (2021), 118129.

[31] Q. Liu, S. Jiang, X. Su, X. Zhang, W. Cao, Y. Xu, Role of the biochar modified with $ZnCl_2$ and $FeCl_3$ on the electrochemical degradation of nitrobenzene, Chemosphere 275 (2021), 129966.

[32] W. Chen, R. Parette, J. Zou, F.S. Cannon, B.A. Dempsey, Arsenic removal by iron-modified activated carbon, Water Res. 41 (2007) 1851–1858.

[33] Y. Hu, Y. Zhu, Y. Zhang, T. Lin, G. Zeng, S. Zhang, Y. Wang, W. He, M. Zhang, H. Long, An efficient adsorbent: simultaneous activated and magnetic ZnO doped biochar derived from camphor leaves for ciprofloxacin adsorption, Bioresour. Technol. 288 (2019), 121511.

[34] X. Zhu, Y. Liu, G. Luo, F. Qian, S. Zhang, J. Chen, Facile fabrication of magnetic carbon composites from hydrochar via simultaneous activation and magnetization for triclosan adsorption, Environ. Sci. Technol. 48 (2014) 5840–5848.

[35] D. Huang, Q. Zhang, C. Zhang, R. Wang, R. Deng, H. Luo, T. Li, J. Li, S. Chen, C. Liu, Mn doped magnetic biochar as persulfate activator for the degradation of tetracycline, Chem. Eng. J. 391 (2020), 123532.

[36] J.-D. Xiao, L.-G. Qiu, X. Jiang, Y.-J. Zhu, S. Ye, X. Jiang, Magnetic porous carbons with high adsorption capacity synthesized by a microwave-enhanced high temperature ionothermal method from a Fe-based metal-organic framework, Carbon 59 (2013) 372–382.

[37] X. Rong, M. Xie, L. Kong, V. Natarajan, L. Ma, J. Zhan, The magnetic biochar derived from banana peels as a persulfate activator for organic contaminants degradation, Chem. Eng. J. 372 (2019) 294–303.

[38] H. Peng, P. Gao, G. Chu, B. Pan, J. Peng, B. Xing, Enhanced adsorption of Cu(II) and Cd(II) by phosphoric acid-modified biochars, Environ. Pollut. 229 (2017) 846–853.

[39] Y. Pan, X. Liu, W. Zhang, B. Shao, Z. Liu, Q. Liang, T. Wu, Q. He, J. Huang, Z. Peng, Y. Liu, C. Zhao, Bifunctional template-mediated synthesis of porous ordered g-C3N4 decorated with potassium and cyano groups for effective photocatalytic H2O2 evolution from dual-electron O2 reduction, Chem. Eng. J. 427 (2022), 132032.

[40] S. Yan, X. Zhang, Y. Shi, H. Zhang, Natural Fe-bearing manganese ore facilitating bioelectro-activation of peroxymonosulfate for bisphenol A oxidation, Chem. Eng. J. 354 (2018) 1120–1131.

[41] M.Z. Afzal, X.-F. Sun, J. Liu, C. Song, S.-G. Wang, A. Javed, Enhancement of ciprofloxacin sorption on chitosan/biochar hydrogel beads, Sci. Total Environ. 639 (2018) 560–569.

[42] W. Yan, R. Zhang, F. Ji, C. Jing, Deciphering co-catalytic mechanisms of potassium doped g-C3N4 in Fenton process, J. Hazard. Mater. 392 (2020), 122472.

[43] M. Pu, Y. Ma, J. Wan, Y. Wang, M. Huang, Y. Chen, Fe/S doped granular activated carbon as a highly active heterogeneous persulfate catalyst toward the degradation of Orange G and diethyl phthalate, J. Colloid Interface Sci. 418 (2014) 330–337.

[44] T. Yamashita, P. Hayes, Analysis of XPS spectra of Fe^{2+} and Fe^{3+} ions in oxide materials, Appl. Surf. Sci. 254 (2008) 2441–2449.

[45] J. Xu, X. Zhang, C. Sun, J. Wan, H. He, F. Wang, Y. Dai, S. Yang, Y. Lin, X. Zhan, Insights into removal of tetracycline by persulfate activation with peanut shell biochar coupled with amorphous Cu-doped FeOOH composite in aqueous solution, Environ. Sci. Pollut. Res. 26 (2019) 2820–2834.

[46] F. Deng, L. Zhao, X. Luo, S. Luo, D.D. Dionysiou, Highly efficient visible-light photocatalytic performance of Ag/$AgIn_5S_8$ for degradation of tetracycline hydrochloride and treatment of real pharmaceutical industry wastewater, Chem. Eng. J. 333 (2018) 423–433.

[47] T. Zhang, H. Zhu, J.-P. Croué, Production of sulfate radical from peroxymonosulfate induced by a magnetically separable CuFe2O4 spinel in water: efficiency, stability, and mechanism, Environ. Sci. Technol. 47 (2013) 2784–2791.

[48] A. Rastogi, S.R. Al-Abed, D.D. Dionysiou, Sulfate radical-based ferrous–peroxymonosulfate oxidative system for PCBs degradation in aqueous and sediment systems, Appl. Catal. B Environ. 85 (2009) 171–179.

[49] H. Meng, C. Nie, W. Li, X. Duan, B. Lai, Z. Ao, S. Wang, T. An, Insight into the effect of lignocellulosic biomass source on the performance of biochar as persulfate activator for aqueous organic pollutants remediation: epicarp and mesocarp of citrus peels as examples, J. Hazard. Mater. 399 (2020), 123043.

[50] J. Yu, L. Tang, Y. Pang, G. Zeng, J. Wang, Y. Deng, Y. Liu, H. Feng, S. Chen, X. Ren, Magnetic nitrogen-doped sludge-derived biochar catalysts for persulfate activation: internal electron transfer mechanism, Chem. Eng. J. 364 (2019) 146–159.

[51] H. Fu, S. Ma, P. Zhao, S. Xu, S. Zhan, Activation of peroxymonosulfate by graphitized hierarchical porous biochar and MnFe2O4 magnetic nanoarchitecture for organic pollutants degradation: structure dependence and mechanism, Chem. Eng. J. 360 (2019) 157–170.

[52] J. Yan, L. Han, W. Gao, S. Xue, M. Chen, Biochar supported nanoscale zerovalent iron composite used as persulfate activator for removing trichloroethylene, Bioresour. Technol. 175 (2015) 269–274.

[53] P. Ntzoufra, J. Vakros, Z. Frontistis, S. Tsatsos, G. Kyriakou, S. Kennou, I. D. Manariotis, D. Mantzavinos, Effect of sodium persulfate treatment on the

physicochemical properties and catalytic activity of biochar prepared from spent malt rootlets, J. Environ. Chem. Eng. 9 (2021), 105071.

[54] J. Wang, S. Wang, Activation of persulfate (PS) and peroxymonosulfate (PMS) and application for the degradation of emerging contaminants, Chem. Eng. J. 334 (2018) 1502–1517.

[55] J. Cao, Z. Xiong, B. Lai, Effect of initial pH on the tetracycline (TC) removal by zero-valent iron: adsorption, oxidation and reduction, Chem. Eng. J. 343 (2018) 492–499.